

Article

# The Effect of Sequential Excitations on Asymmetrical Reinforced Concrete Low-Rise Framed Structures

Paraskevi K. Askouni 

Department of Civil Engineering, University of Patras, 26504 Rio, Greece; askounie@upatras.gr

**Abstract:** In the current research, the elastoplastic behaviour of symmetrical and asymmetrical reinforced concrete buildings is explored by dynamic analysis. The used ground excitations are of sequential type, which is found in the literature to possibly strongly affect the dynamic structural behaviour. The contemporary seismic codes neglect the impact of sequential earthquakes on the seismic response, highlighting a scientific gap necessary to be studied. Within the scope of this study, ordinary 3D reinforced concrete low-rise building frames are forced to sequential ground excitations, as well as to a respective single-occurrence corresponding ground excitation, for comparability reasons. In the present dynamic analyses, the two horizontal directions of the excitations, along with the vertical one, are included in the analysis input. The nonlinear behaviour of reinforced concrete sections under strong strain is considered in the present analyses. The geometrical in-plan asymmetry of the 3D models is expressed by a simply defined ratio. Selected unitless resulting plots of the current dynamic analyses are presented and appropriately discussed given the relative geometrical asymmetry. The role of sequential ground excitations on the dynamic response is recognized, along with the role of simple geometrical symmetry or asymmetry, in the resulting response plots. Thus, useful conclusions are acquired, pointing to remarks on the geometrical structural design helpful for the development of recommendations of seismic provisions.

**Keywords:** symmetry; asymmetry; sequential earthquake; reinforced concrete; time history analysis; elastoplastic behaviour



**Citation:** Askouni, P.K. The Effect of Sequential Excitations on Asymmetrical Reinforced Concrete Low-Rise Framed Structures. *Symmetry* **2023**, *15*, 968. <https://doi.org/10.3390/sym15050968>

Academic Editor: Gennadiy Kolesnikov

Received: 12 April 2023

Revised: 21 April 2023

Accepted: 22 April 2023

Published: 24 April 2023



**Copyright:** © 2023 by the author. Licensee MDPI, Basel, Switzerland. This article is an open access article distributed under the terms and conditions of the Creative Commons Attribution (CC BY) license (<https://creativecommons.org/licenses/by/4.0/>).

## 1. Introduction

The geometrical symmetry/asymmetry of buildings is already reported to have an impact on the seismic response in studies in the literature, such as in Bento et al. [1]. Alongside that, various studies can be found on the nonlinear analysis of buildings by reinforced concrete (RC), which is within the current field of investigation, mainly involving the typical rigid base assumption as usually considered for the earthquake design of common building structures by the current Eurocode 8 (EC8) [2]. Indicatively, some similar research articles are mentioned, such as the state-of-the-art review conducted by Rutenberg [3], where the effect of in-plan building asymmetry on the nonlinear response was recognized and synthetically compared to the code assumptions and case studies. Das et al. [4] critically summarized various research investigations and code assumptions on the performance of asymmetric and irregular buildings, showing that more future research is necessary for the understanding of the response effect of bidirectional ground motions. The modification of internal forces was investigated in one-storey 2D asymmetrical reinforced concrete frames under a synthetic earthquake, comparing the frame response for the common rigid soil assumption and a flexible ground [5]. Asymmetrical 3D RC frames were forced to strong ground excitations, providing a response comparison for the boundary ground conditions, i.e., rigid ground or deformable ground [6]. The elastoplastic behaviour of reinforced concrete buildings was found to be altered because of the ground deformability, as in [7].

The applicable seismic provisions neglect sequential earthquakes' influence on the structural response, which is obvious in some literature articles, as mentioned as follows. The impact of "core-wall" [8] systems on the structural stability regarding the

torsion of asymmetric multi-storey reinforced concrete framed buildings are investigated by Xing et al. [8]. Hatzigeorgiou and Beskos [9] have proposed estimated numerical ratios for the ratio of nonlinear displacement of a simple 1D model under repeated earthquakes. In a further in-depth study of the effect of multiple earthquakes, Hatzigeorgiou [10] proposed behavioural factors for corresponding nonlinear structures and presented spectra for the ductility demand concerning simple models under these earthquakes [11]. The influence of seismic sequences on RC irregular-in-height buildings was investigated in 2D conditions by Hatzigeorgiou and Liolios [12] and in 3D conditions by Hatzigeorgiou and Hatzivasiliou [13]. Lazaridis et al. [14] investigated a 2D building model based on [12] by using algorithms for machine learning to predict structural damage under seismic sequences.

Concerning structures constructed not only by reinforced concrete but other materials, or even more complex and non-ordinary structures under sequential earthquakes, there are some research articles available in the literature, as indicatively given here. The effect of sequential earthquakes on 2D steel frames was studied by “incremental dynamic analysis” [15]. The sensitivity of a real existing RC building case with masonry infills was examined by nonlinear time history (NLTH) analyses under seismic sequences by Mahat et al. [16]. Frames by reinforced concrete supplied with extra damper columns were subjected to seismic consequences by Fujii [17], employing NLTH analyses to highlight the influence of the added damper. Konstantakopoulou et al. [18] studied the dynamic response of jacket platforms under multiple earthquakes in 3D conditions, comparing the common rigid soil assumption to a flexible ground.

In addition, the direction of the earthquake motion is recognized to have an impact on the structural response in a range of research articles, mostly considering rigid soil by using global quantities for the assessment of the response outcomes [19–25]. A few works have also considered the soil deformability on the response of RC buildings while regarding a changeable angle of the earthquake direction [5–7]. The aforementioned research works have indicated the most detrimental structural response from the perspective of the earthquake direction.

The present research aims to highlight the effect of a geometrical simple symmetry or asymmetry in-plan of RC common buildings in the 3D space. This symmetry/asymmetry is expressed by unitless parameters, similar to Refs. [5–7]. These reinforced concrete frames are analyzed by NLTH analyses considering multiple ground excitations with various incidences, which are not included in the applicable seismic regulation [2], although their response effect is identified, as previously mentioned [8–17]. In addition, the considered excitations include a single event for comparison purposes of the response results. The NLTH analyses are preferred here due to providing greater accuracy of results, though being more demanding in computing power and time [26], as well as needing a large number of accelerograms [2], among other aspects. The assessment of the elastoplastic response outcomes is based on general response ratios while using a dimensionless simple ratio to account for the geometrical symmetry/asymmetry of the reinforced concrete building frames.

## 2. Considered RC Buildings and Methodology

Simple low-rise 3D RC one- and three-storey small-size buildings are currently forced to sequential earthquakes by nonlinear time history analyses. In the initial stage, 1-storey RC frames are investigated, with a height of 4.0 m consisting of 1 RC slab with dimensions  $5.0 \times 4.0 \text{ m}^2$ , a thickness of 15 cm, and a considered diaphragm action. This RC slab rests on 4 perimeter reinforced concrete beams with a  $25 \times 60 \text{ cm}^2$  cross-section and 4 RC columns, each at the in-plan corners (Figure 1). The 3 columns have an invariable cross-section of  $40 \times 40 \text{ cm}^2$ . The cross-section of one column, called “wall” in the current work, varies from  $40 \times 40 \text{ cm}^2$ , as in Figure 1a, up to  $30 \times 200 \text{ cm}^2$ , as in Figure 1b. Thus, in this way, the geometrical in-plan asymmetry of the 3D 1-storey RC buildings is induced.

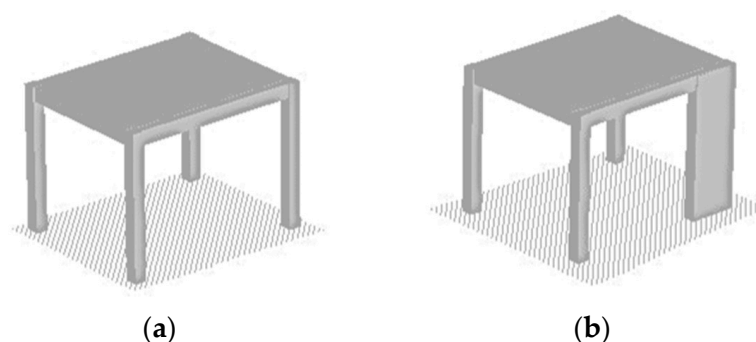


**Figure 1.** (a) Symmetrical and (b) asymmetrical RC one-storey buildings considered.

Afterwards, similar three-storey buildings are formed (Figure 2), with their first storey the same as the one-storey frames. The 2nd and 3rd storeys of the 3-storey buildings are similar to the 1st one, with a floor level 3.0 m over the 1st storey. The 3 columns of the 2nd and 3rd storeys have an invariable cross-section equal to  $35 \times 35 \text{ cm}^2$ , while 1 column, referred to here as “wall”, has an in-steps-increasing cross-section from  $35 \times 35 \text{ cm}^2$  up to  $30 \times 200 \text{ cm}^2$ , introducing the in-plan asymmetry, as previously mentioned in the 1-storey frames. The beam cross-section is invariable at  $25 \times 60 \text{ cm}^2$  in the 1-storey and all storeys of the 3-storey buildings. The slabs of the 3-storey 3D framed buildings have a thickness of 15 cm acting as rigid diaphragms.

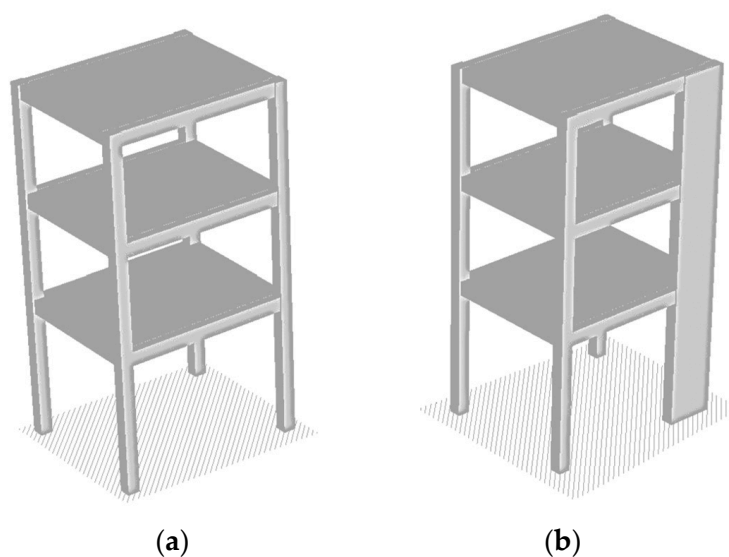


**Figure 2.** Considered three-storey (a) symmetrical and (b) asymmetrical RC buildings.

The structural members are made of reinforced C20/25 with steel type B500c, which is typical for common low-rise buildings. The buildings are designed to conform to the current codes [2,27] as ordinary buildings for domestic and residential activity areas with 1.0 as the considered importance factor. The slab loading consists of a permanent load of  $2.0 \text{ kN/m}^2$  and a moving load of  $0.6 \text{ kN/m}^2$  [28]. A wall dead load of  $3.6 \text{ kN/m}^2$  (per wall height) is utilized upon the beams [28]. The RC building frames are seismically designed for a ductility class medium (DCM) and the common inflexible ground assumption [2] considering the rule of “capacity design” [2,27] of joints and members against shear [2] (Figure 3). The seismic design considerations following the guidelines of [2] are zone ground acceleration of  $0.36 \text{ g}$ , a type 1 design spectrum, a 5% ratio of viscous damping, C type of soil, and the estimated “behaviour factor” by [2] for each building case. The seismic design combinations include the 30% guideline and the “accidental eccentricity” of 5% [2]. Due to the current study on the response of common small, framed structures with

the perspective of simple geometrical symmetry or asymmetry, the possible effect of soil deformability is neglected here [2].

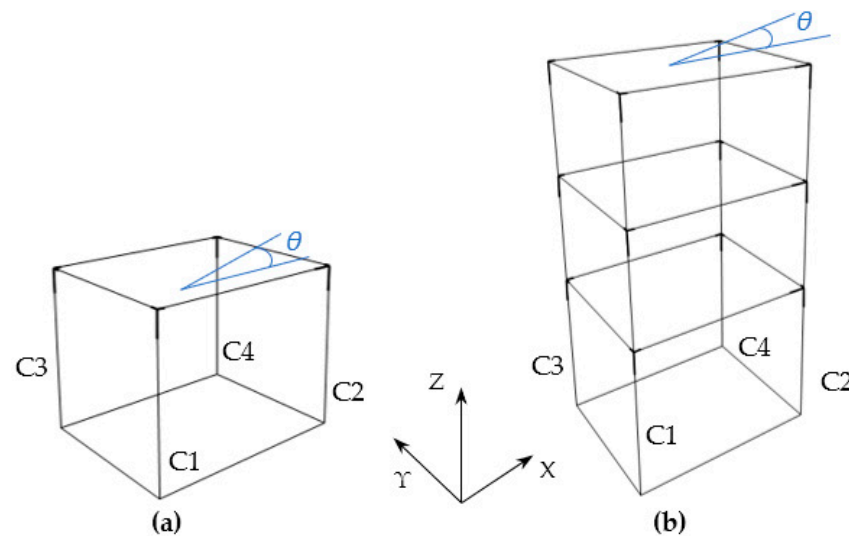


**Figure 3.** Models of the (a) one- and (b) three-storey considered framed structures with the global coordinate system and angle of incidence of the earthquake.

The current investigation considers five sequential ground motions in the 3D space as follows: the excitation of “Chalfant Valley” [29], in 1986, consisting of 2 single seismic events; the excitation of “Coalinga” [29], in 1983, consisting of 2 single occurrences; the excitation of “Imperial Valley” [29], in 1979, by 2 single occurrences; the excitation of “Mammoth Lakes” [29], in 1980, by 5 single occurrences; and the excitation of “Whittier Narrows” [29], in 1987, by 2 single occurrences. The ground acceleration data are downloaded by [29] and indicatively plotted in Figure 4 for the most intense horizontal direction. Between two subsequent seismic occurrences of each considered ground excitation, a time frame of 100 s is applied with 0.0 values of the excitation input to conciliate the building vibration due to damping, following the method of Refs. [9–13].

For comparison purposes of the possible effect of multiple ground excitations to a single one, the 3D buildings are also subjected to the 1st part of the Mammoth Lakes earthquake, as shown in Figure 4d, which is noticed in the time frame of 0–50 s of the respective accelerogram and called here “Mammoth-1st”. Indicatively, for the whole Mammoth Lakes earthquake, the maximum ground accelerations are  $4.332 \text{ m/s}^2$  and  $4.086 \text{ m/s}^2$  in the horizontal orientation and  $3.807 \text{ m/s}^2$  in the vertical one, which coincide with the maximum observed values for the 1st part of the Mammoth Lakes earthquake.

The earthquake incidence angle is shown in the available literature to affect the structural response, as previously mentioned [21–25]. In the current analyses with a basis on the shape plan of the examined buildings, the chosen angles of the direction of the earthquakes are  $\theta = 0^\circ$ ,  $\theta = 90^\circ$ , and  $\theta = 45^\circ$ , which are, respectively, parallel to the two horizontal geometrical axes (Figure 3) and close to the geometrical diagonal axis.

The dynamic analyses of the investigated structures are accomplished by ETABS [30] considering the nonlinear behaviour of RC members, i.e., elastic under low loading and plastic under strong/extreme burdening conditions. Consequently, at the structural component ends, elastoplastic point hinges are applied, integrating the main characteristics of interest according to the guidelines of [31,32], such as geometrical features, material quality, sectional detailing, strength mechanical limits, reduced stiffness, limit bending moments, limit curvature, and plastic chord rotation angles. In addition, a potential weakness in the shear of RC sections is assessed, complying with the guidelines of [2,27,33].

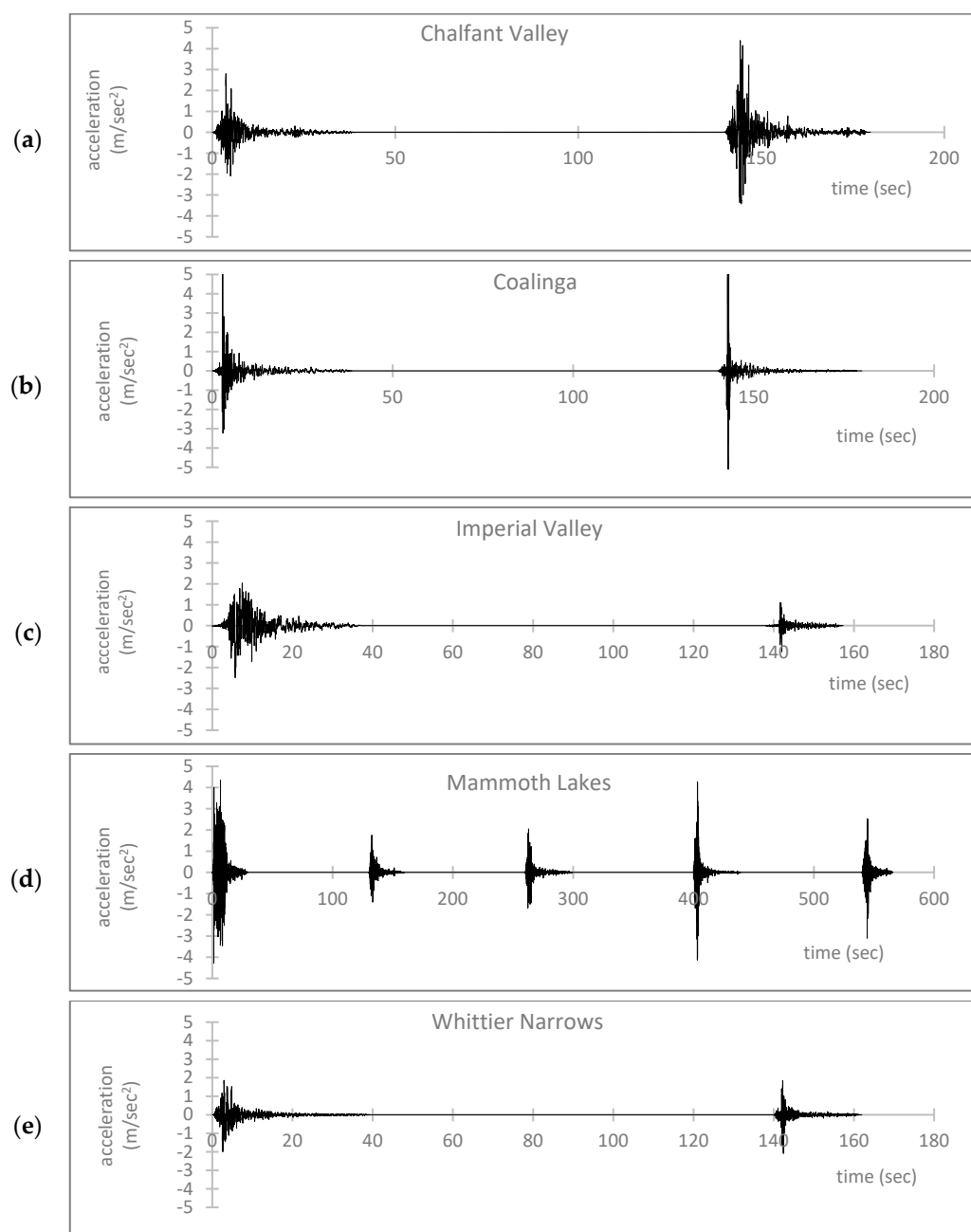


**Figure 4.** Ground acceleration data of the considered sequential earthquakes: (a) Chalfant Valley, (b) Coalinga, (c) Imperial Valley, (d) Mammoth Lakes, and (e) Whittier Narrows.

### 3. Structural Results and Discussion

The NLTH analyses of outcomes considering sequential earthquakes in 3D conditions are evaluated by appropriate parameters and discussed here. The simple geometrical asymmetry induced in the investigated 3D models involves the comparative symmetry or asymmetry of the structural columns in terms of cross-section and stiffness, numerically expressed here by the numerical division of the wall section to the column one, giving the so-called “A-ratio”.

Through modal analysis [34] of the considered 3D models performed by ETABS [30], the modal characteristics are obtained. The modal periods of the three important modes are presented for each building in the following Table 1. In the spectra of the considered earthquakes, the fundamental mode of the examined buildings is depicted for evaluation of the diagrams by vertical lines with grey colour (Figures 5 and 6). As observed in Figure 5a,

the fundamental mode of the one-storey buildings is near the widest spectrum range of values in the horizontal direction [2], as well as to the greatest range of the Chalfant Valley spectrum. The spectra of the regarded seismic sequences are relatively close to the design spectrum [2], so these are considered appropriate for the current investigation.

**Table 1.** Fundamental modal periods of the studied buildings.

| Dimensions of the Wall (cm/cm) | One-Storey Buildings |              | Three-Storey Buildings |            |
|--------------------------------|----------------------|--------------|------------------------|------------|
|                                | Mode                 | Period (sec) | Mode                   | Period (s) |
| 40/40                          | 1                    | 0.528        | 1                      | 1.082      |
|                                | 2                    | 0.511        | 2                      | 1.047      |
|                                | 3                    | 0.475        | 3                      | 0.965      |
| 70/30                          | 1                    | 0.564        | 1                      | 1.125      |
|                                | 2                    | 0.501        | 2                      | 1.04       |
|                                | 3                    | 0.441        | 3                      | 0.901      |
| 100/30                         | 1                    | 0.542        | 1                      | 1.076      |
|                                | 2                    | 0.495        | 2                      | 1.014      |
|                                | 3                    | 0.4          | 3                      | 0.814      |
| 125/30                         | 1                    | 0.511        | 1                      | 1.028      |
|                                | 2                    | 0.489        | 2                      | 1.0        |
|                                | 3                    | 0.356        | 3                      | 0.782      |
| 150/30                         | 1                    | 0.503        | 1                      | 1.016      |
|                                | 2                    | 0.484        | 2                      | 0.992      |
|                                | 3                    | 0.323        | 3                      | 0.693      |
| 175/30                         | 1                    | 0.498        | 1                      | 1.007      |
|                                | 2                    | 0.48         | 2                      | 0.984      |
|                                | 3                    | 0.296        | 3                      | 0.636      |
| 200/30                         | 1                    | 0.493        | 1                      | 1.007      |
|                                | 2                    | 0.473        | 2                      | 0.986      |
|                                | 3                    | 0.271        | 3                      | 0.699      |

Selected plots of the “interstorey drift ratio” (“IDR”) [33] on each storey of the 3D buildings are presented in comparison to the “performance levels” [35] limitations, which are indicated for reading ease concerning RC frames: 1% for the “Immediate Occupancy” (“IO”) [35] level, 2% for the “Life Safety” (“LS”) [35] level, and 4% for the “Collapse Prevention” (“CP”) [35] level. Additionally, diagrams for the residual IDR (RIDR) are presented compared to the RIDR limits of [35], which are negligible for the “IO” level, 1% for the “LS” level, and 4% for the “CP” level. In addition, plots of the “ratio of the peak floor acceleration to the peak ground acceleration” (“PFA/PGA”) [36] are given to assess the nonlinear structural response, although respective limit values do not exist in the literature. In the following plots, each earthquake is followed by the value of the respective incidence angle. The plots of dimensionless parameters are preferred in the current investigation to provide more objective remarks and conclusions.

The nonlinear behaviour of the reinforced concrete elements is checked by coloured notations at the hinges of the element ends, following the recent code provisions where these letters are used: “A” [30] indicates the elastic behaviour of the RC section [2,27,33], “B” [30] indicates the “yielding bending moment” [2,27,33], “C” [30] is for the ultimate yielding bending moment [2,27,33], “D” [30] is for the “residual bending moment limit” [2,27,33], and “E” [30] indicates bending moments over the previous limits and deformations over the ultimate deformation limit [2,27,33,37]. These mentioned necessary limits are inserted in the analysis model through the aforementioned properties of the elastoplastic hinges, as calculated by [31–33]. Due to lack of space, the most detrimental diagrams of the seismic structural response are presented as follows.

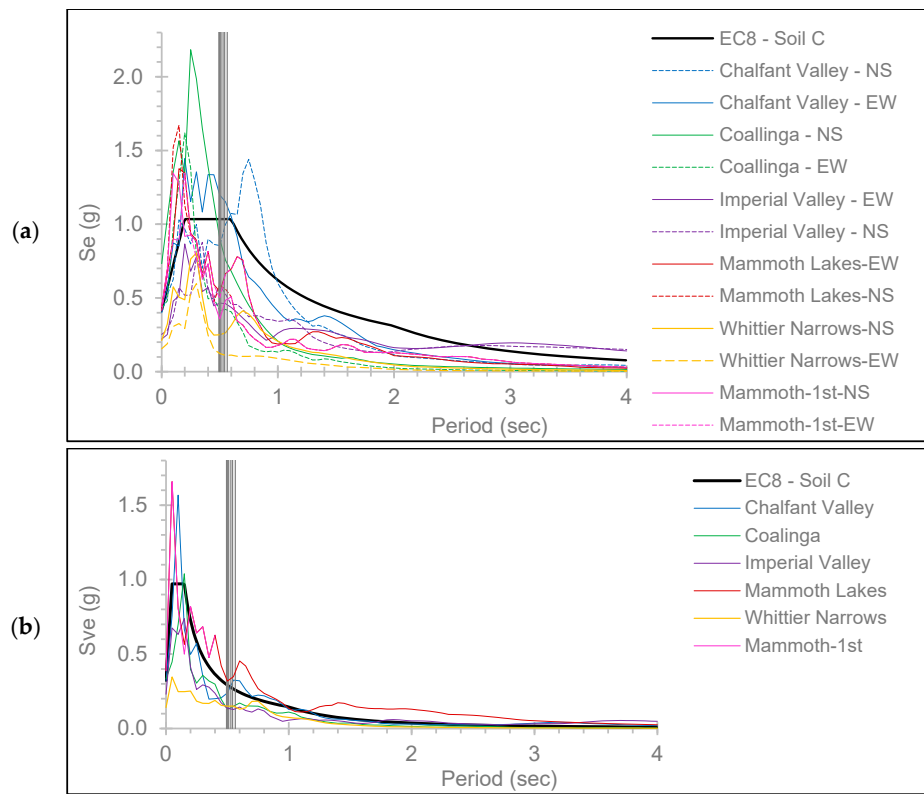


**Figure 5.** Compatibility check of the considered earthquakes to the code spectrum in comparison to 1st mode of 1-storey structures (a) in the horizontal directions and (b) vertical direction.

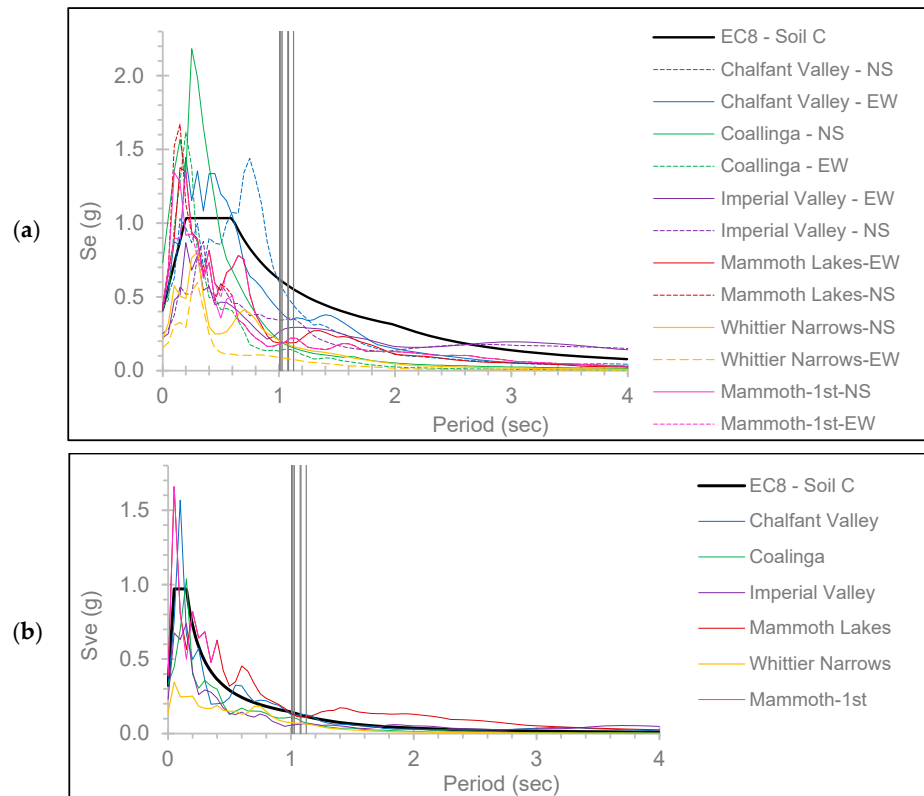


**Figure 6.** Compatibility check of the considered earthquakes to the code spectrum in comparison to 1st mode of 3-storey structures (a) in the horizontal directions and (b) vertical direction.

### 3.1. Comments on the One-Storey Structures

For the one-storey RC buildings, the IDR-X with  $\theta = 0^\circ$  decreases along with an increase in the A-ratio, as shown in Figure 7a, where greater values are noted for the “Chalfant Valley” earthquake with a range of 0.9%~1.4% within the limit of the LS performance level [35]. The IDR-X for Mammoth Lakes and  $\theta = 0^\circ$  (Figure 7a) decreases variably for greater values of the A-ratio in the range of 0.6%~0.81%, while for the Mammoth-1st, there are decreases in the range of 0.38%~0.69%, within the limit of the IO performance level [35].

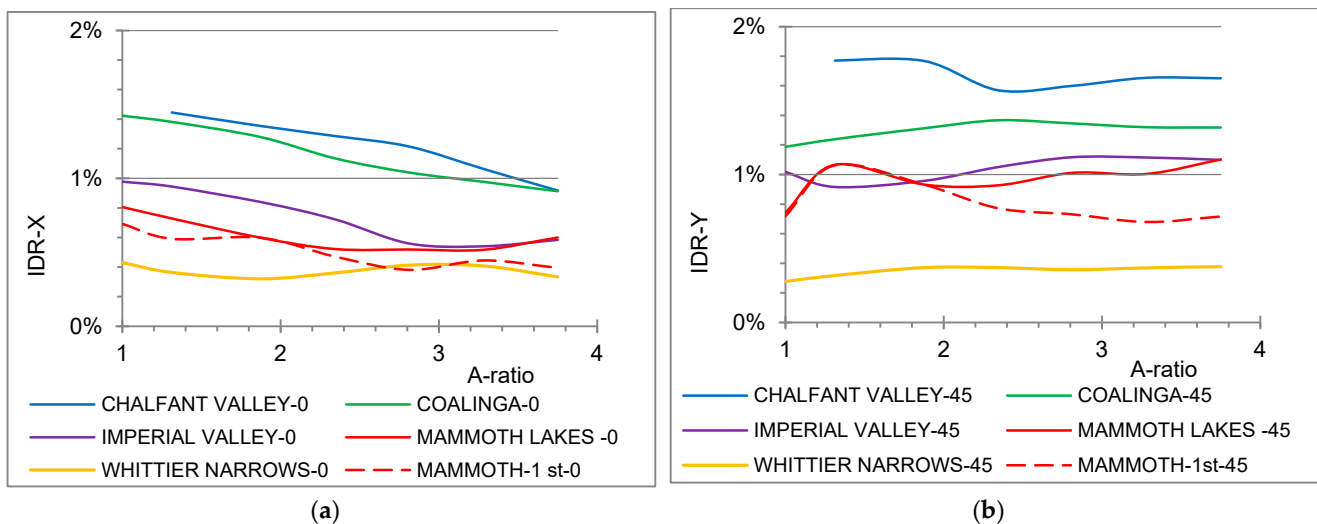


Figure 7. (a) IDR-X axis,  $\theta = 0^\circ$ ; (b) IDR-Y,  $\theta = 45^\circ$ .

The IDR-Y with  $\theta = 45^\circ$  (Figure 7b) varies in the range of 0.38%~1.77%, within the limit of the LS performance level [35], where greater values are observed for the Chalfant Valley earthquake and smaller ones for the Whittier Narrows, similarly to the IDR-X plot,  $\theta = 0^\circ$ . The IDR-Y values for the Mammoth-1st strong ground motion and  $\theta = 45^\circ$  vary along with a greater A-ratio in a range of values that are 28%~35% smaller than the respective one for the Mammoth Lakes earthquake for an A-ratio  $\geq 2.34$  (Figure 7b). The discontinuity of the IDR plotline (Figure 7a,b) for the symmetrical building for the Chalfant Valley earthquake with  $\theta = 0^\circ$  and  $\theta = 45^\circ$  indicates building failure due to deformations much higher than the limits of [35], which complies with the observations for the earthquake spectra in Figure 5.

For comparison purposes, in Figure 8, the IDR plots for  $\theta = 90^\circ$  are presented concerning both horizontal axes. The IDR-X tends to decrease for all earthquakes with an increase in the A-ratio, showing, in general, a value range of 0.2~1.4%, within the LS level [35] (Figure 8a). The IDR-Y varies with a small increasing tendency for greater A-ratios, (Figure 8b) in the range of 0.4%~1.9%, within the LS level [35] (Figure 8b). The IDR-X tends to have values for the Mammoth-1st excitation that are similar to the whole Mammoth Lakes earthquake by a mean percentage in the X-axis (Figure 8a). However, the IDR-Y has smaller values for the Mammoth-1st compared to the whole Mammoth Lakes earthquake by up to 29% for the biggest wall section (Figure 8b). The greatest IDR-Y values tend to be greater than the respective ones of IDR-X by a mean percentage of 29% (Figure 8a,b). Among the considered earthquakes, greater IDR values are observed for the Chalfant Valley earthquake and the Coalinga earthquake and smaller IDR values for the Whittier Narrows earthquake (Figures 7 and 8).

The RIDR-X with  $\theta = 0^\circ$  (Figure 9a) decreases variably in the value range of 0.01%~0.39% for an A-ratio  $\leq 2.34$  and increases for bigger wall sections to 0.002%~0.17%, i.e., presenting a general value range within the limit of the LS performance level [35]. As presented in Figure 9b, the RIDR-Y with  $\theta = 45^\circ$  varies 0~0.46% within the limit of the LS performance level [35]. In Figure 9a,b, greater values tend to be observed for the earthquake of Chalfant Valley than the other earthquakes. The values of the plotline of Figure 9b for the

Mammoth-1st tend to be smaller by 38%~41% than the values for the entire Mammoth Lakes earthquake.

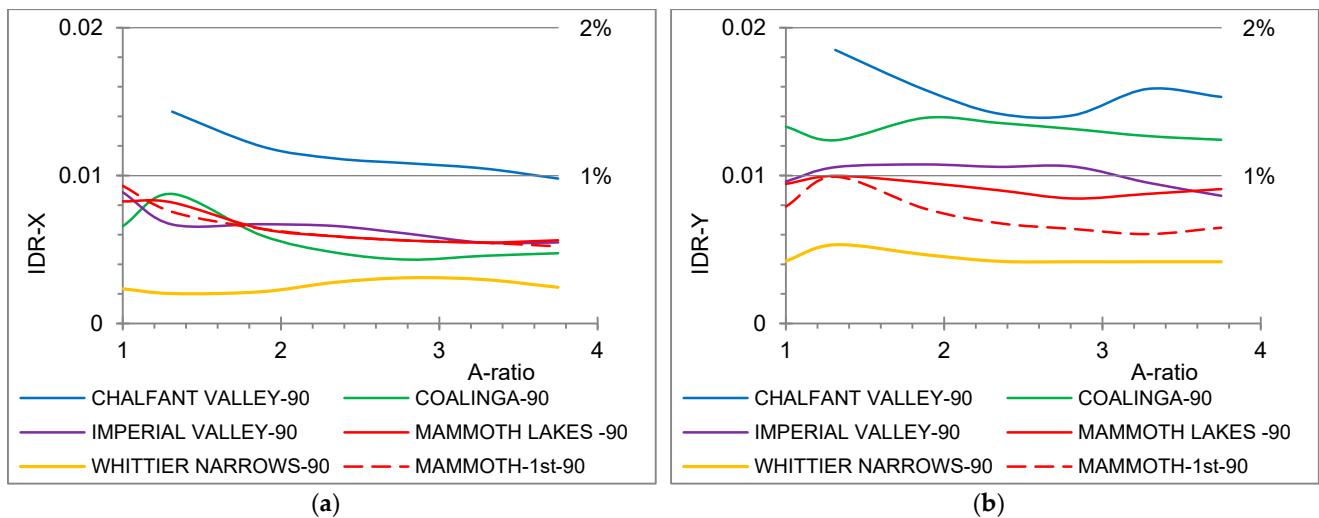


Figure 8. (a) IDR-X axis,  $\theta = 90^\circ$ ; (b) IDR-Y axis,  $\theta = 90^\circ$ .

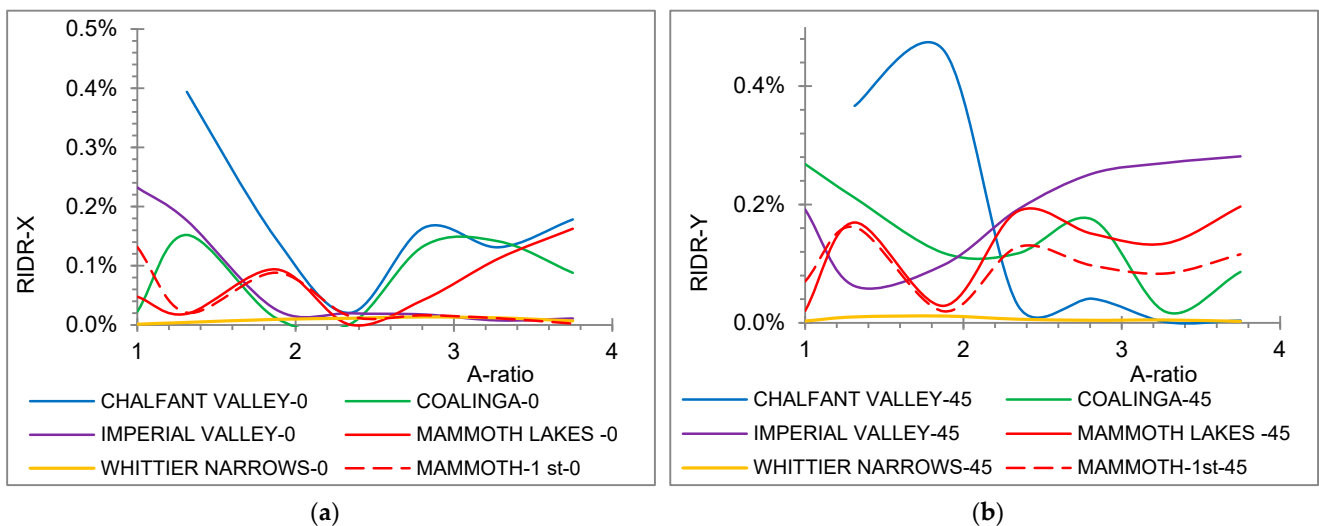


Figure 9. (a) RIDR-X axis,  $\theta = 0^\circ$ ; (b) RIDR-Y axis,  $\theta = 45^\circ$ .

The PFA/PGA on the X-axis with  $\theta = 90^\circ$  is observed in Figure 10a to increase for bigger A-ratios with a value field up to 2.56~4.52 regarding the highest wall section. The PFA/PGA-Y with  $\theta = 45^\circ$  (Figure 10b) increases up to 2.25~4.38 for the maximum wall section. In Figure 10a,b, the PFA/PGA presents a bigger range for the Imperial Valley excitation in comparison to the rest. The values of the plots of Figure 10 for the Mammoth-1st tend to be slightly smaller by 7~8% than the values for the entire Mammoth Lakes earthquake for greater wall sections. In Figures 9 and 10, the gap of the plotline for the Chalfant Valley earthquake represents building failure for this earthquake, noticed similarly to previous plots.

Concerning the one-storey symmetrical model (Figure 11a,b), the hinge formation is within limit C [35], which is acceptable by the guidelines of current seismic codes. For the Mammoth-1st with  $\theta = 90^\circ$ , as in Figure 11a, the hinges tend to behave nonlinearly within the limits of [1,35]. For the Whittier Narrows with  $\theta = 90^\circ$ , as in Figure 11b, most elements tend to exhibit elastic behaviour.

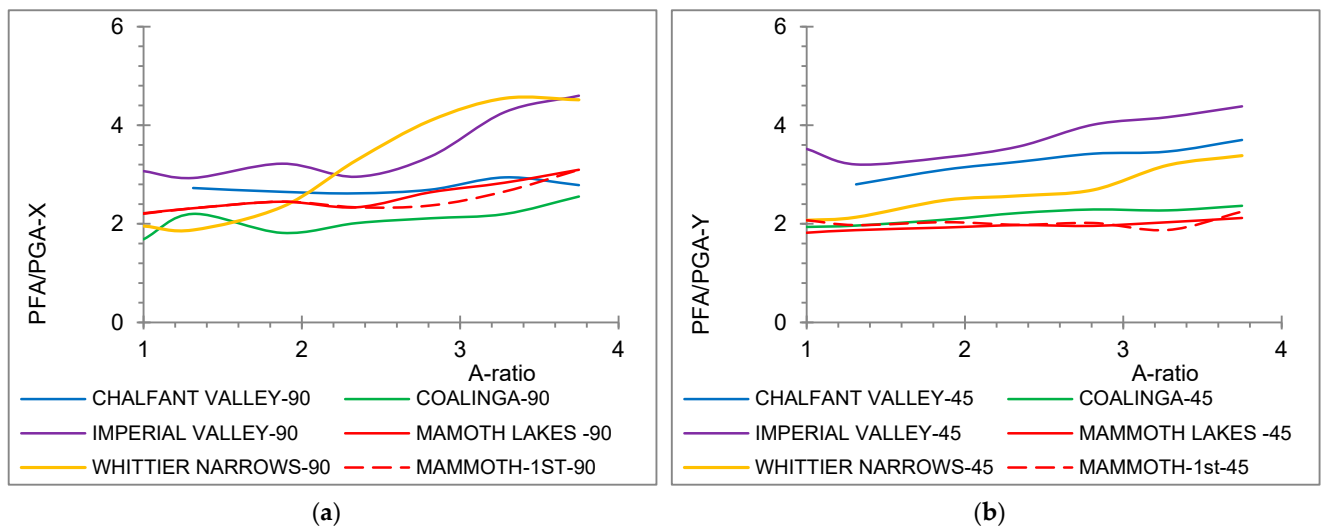


Figure 10. (a) PFA/PGA-X,  $\theta = 90^\circ$ ; (b) PFA/PGA-Y,  $\theta = 45^\circ$ .

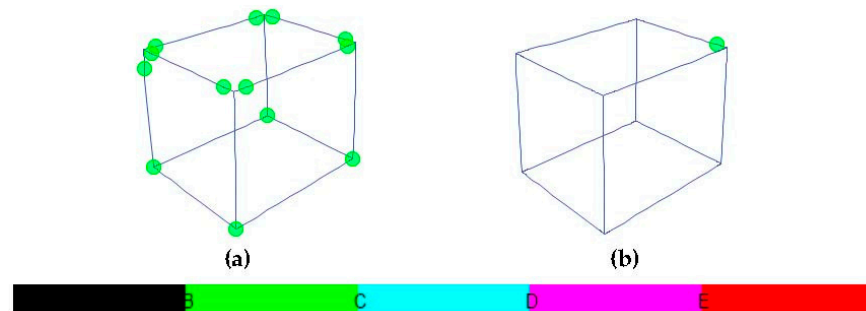


Figure 11. Hinge formation for the one-storey symmetric framed structure regarding (a) Mammoth-1st with  $\theta = 90^\circ$  and (b) Whittier Narrows with  $\theta = 90^\circ$ .

For the one-storey asymmetrical buildings, as presented in Figures 12 and 13, the hinge formation is within the code limitations [1,35]. Indicatively, for the one-storey frame with the 150/30 cm wall, the worst hinge formation is observed for Chalfant Valley with  $\theta = 0^\circ$ , as in Figure 12a, and the most beneficial hinge formation is observed for the Whittier Narrows earthquake with  $\theta = 45^\circ$  (Figure 12a). For the one-storey framed model with the maximum wall section, i.e., 200/30 cm, the worst formation of elastoplastic hinges is presented in Figure 13b, still within the C limit, for the Coalinga earthquake with  $\theta = 0^\circ$ , and the most beneficial one is shown in Figure 13c for the Whittier Narrows earthquake with  $\theta = 0^\circ$ .

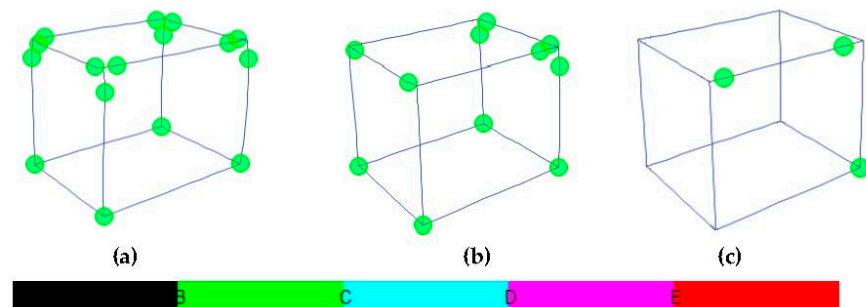
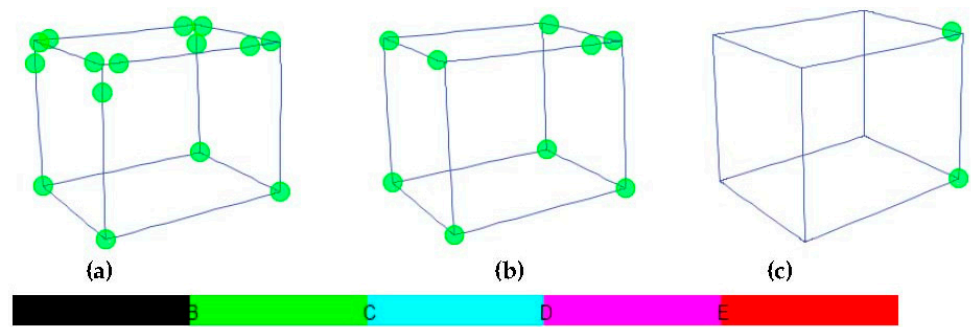


Figure 12. Hinge formation for the one-storey framed structure with 150/30 cm wall section regarding (a) Chalfant Valley with  $\theta = 0^\circ$ , (b) Mammoth Lakes with  $\theta = 0^\circ$ , and (c) Whittier Narrows with  $\theta = 45^\circ$ .



**Figure 13.** Hinge formation for the one-storey framed structure with 200/30 cm wall section regarding (a) Coalinga with  $\theta = 0^\circ$ , (b) Imperial Valley with  $\theta = 45^\circ$ , and (c) Whittier Narrows with  $\theta = 0^\circ$ .

### 3.2. Comments on the Three-Storey Structures

Concerning the 3-storey framed structures, on their 1st storey (Figure 14a) the IDR-X with  $\theta = 90^\circ$  decreases for an A-ratio  $\leq 2.34$  and variably increases for bigger wall sections. More specifically for the Chalfant Valley  $\theta = 90^\circ$  and Imperial Valley  $\theta = 90^\circ$ , the IDR-X decreases for an A-ratio  $\leq 2.34$  in the value range of 1.1%~1.7%, i.e., within the limit of the LS performance level [35]. For the greater wall section with A-ratio = 3.28, the IDR-X is 1.35% concerning the Chalfant Valley with  $\theta = 90^\circ$  and 0.85% for the earthquake of Imperial Valley with  $\theta = 90^\circ$ . For the earthquakes of Coalinga, Mammoth Lakes, and Whittier Narrows with  $\theta = 90^\circ$  (Figure 14a), the IDR-X varies in the range of 0.3%~0.8%, i.e., within the limit of 1% corresponding to the IO performance level [35]. The gaps in the plotlines of Figure 14a represent building failures for these building cases under sequential excitations.

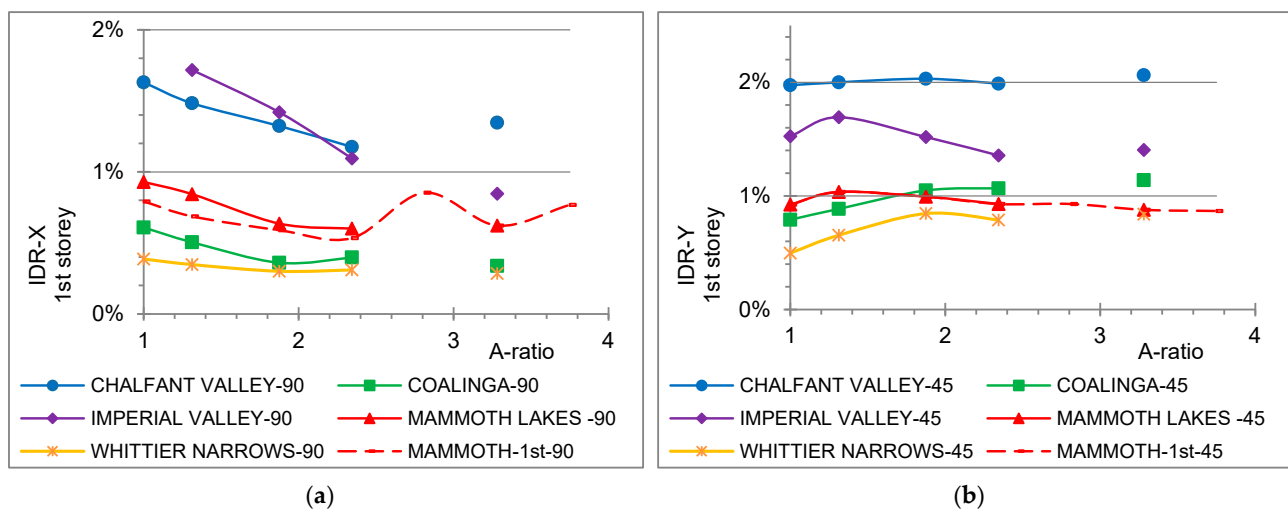


**Figure 14.** (a) IDR-X,  $\theta = 90^\circ$ , and (b) IDR-Y,  $\theta = 45^\circ$ , 1st storey.

As in Figure 14b, at the 1st storey of the 3-storey structures,  $\theta = 45^\circ$ , the IDR-Y varies in the range of 0.5%~2.03% for the examined earthquakes, with bigger values for the Chalfant Valley earthquake and lower ones for the Whittier Narrows earthquake. Similarly to Figure 14a, the gaps in the plotlines of Figure 14b represent building failures due to extreme seismic response deformations, noticed mainly for the wall sections of 150/30 cm and 200/30 cm for the sequential earthquakes. Additionally, in Figure 14b, the IDR plotline of Mammoth-1st is continuously shown, in contrast to the plotline of the Mammoth Lakes sequential earthquake. The latter observation implies a negative impact of the sequential excitations on the seismic response compared to single-event excitation.

At the 2nd storey of the 3-storey RC structures, the IDR-X with  $\theta = 90^\circ$  increases variably with an increase in the A-ratio, as observed in Figure 15a. A bigger value range of IDR-X (Figure 15a) is observed for the Chalfant Valley, as 1.7%~2.1%, which is slightly

over the limit of LS and within the CP performance levels [35]. The smaller value range of Figure 15a is noticed for the Whittier Narrows with  $\theta = 90^\circ$ , as 0.3%~0.5%, within the limit of the IO performance level.

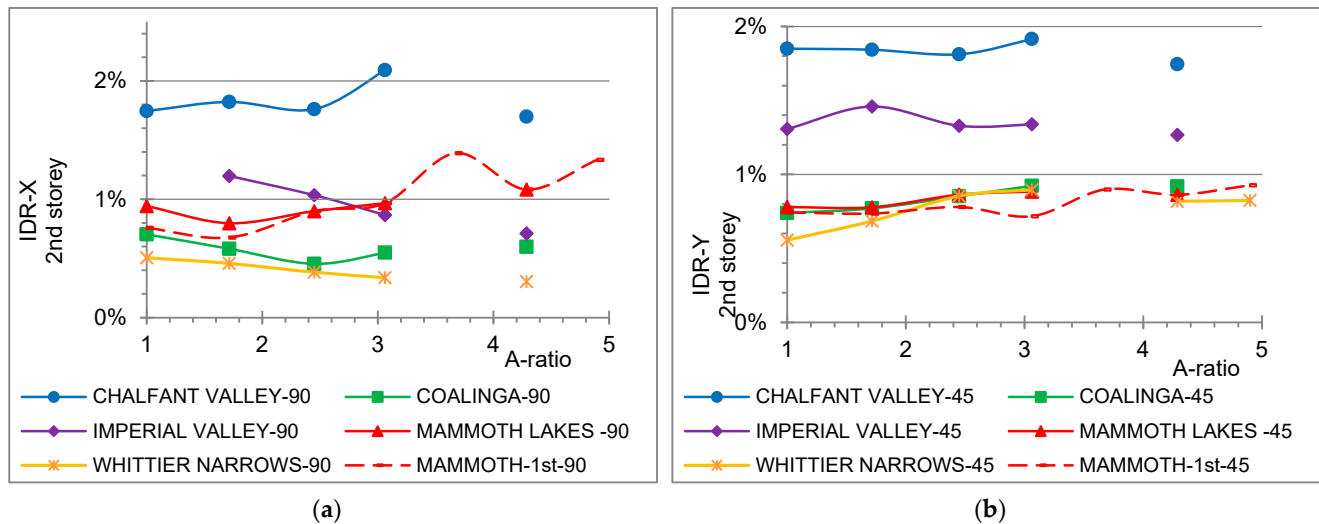


Figure 15. (a) IDR-X,  $\theta = 90^\circ$ , and (b) IDR-Y,  $\theta = 45^\circ$ , 2nd storey.

As in Figure 15b, at the 2nd storey of the 3-storey RC structures, the IDR-Y varies for greater A-ratios in the range of 1.3%~1.9% for the Chalfant Valley and Imperial Valley earthquakes with  $\theta = 45^\circ$ . The IDR-Y for the earthquakes of Coalinga, Mammoth Lakes, Mammoth-1st, and Whittier Narrows, all with  $45^\circ$ , is observed in Figure 15b to vary, slightly increasing for greater values of the A-ratio in the range of 0.5%~0.9%.

At the 3rd storey, as in Figure 16a,b, the IDR-X and IDR-Y axes increase variably for greater A-ratios within the LS performance level [35]. The IDR-X shows in Figure 16a greater values for the earthquake of Coalinga with  $\theta = 0^\circ$  in the range of 1.4%~1.7% and smaller values for the Mammoth-1st with  $\theta = 0^\circ$  in the range of 0.7%~0.8%. The IDR-Y (Figure 16b) has increased values for the Coalinga earthquake with  $\theta = 90^\circ$  up to 1.6% for A-ratio = 3.06 and has a maximum value of 1.8% for A-ratio = 4.29 for the Chalfant Valley earthquake with  $\theta = 90^\circ$ . At the 2nd and 3rd storeys, the results of the NLTH analyses for the cases of A-ratio = 3.67 and A-ratio = 4.89 are not plotted in Figures 15 and 16 due to building failure, as similarly observed in previous plots, for the sequential ground motions. However, for the excitation of Mammoth-1st, the response results are plotted in previous Figures 14–16, despite the building failures of the corresponding sequential earthquake of Mammoth Lakes.

The greater IDR-X values at the 1st storey are 15% lower than the respective ones at the 2nd storey, while a similar range of IDR-X values exists for 3rd and 1st storeys. Maximum IDR-Y values on the 1st storey are higher by 5% compared to the 2nd one and by 20% compared to the 3rd storey. The IDR-X and IDR-Y values at all storeys are within the limits of the performance levels [35].

Concerning the RIDR-X plot  $\theta = 0^\circ$  (Figure 17a) at the 1st storey, the general range of plot values is within the LS performance level [35]. However, in Figure 17a, local increased values up to 0.66% of RIDR-X are observed for the symmetrical building case. For A-ratio = 1.31~2.34, the RIDR-X varies in the range of 0~0.26%. The RIDR-X plotlines are discontinued for A-ratio = 2.81 and A-ratio = 3.75 because of building failure for these cases for the sequential excitations due to extreme response deformations much greater than the upper limits of the performance levels [35], similar to previous figures.

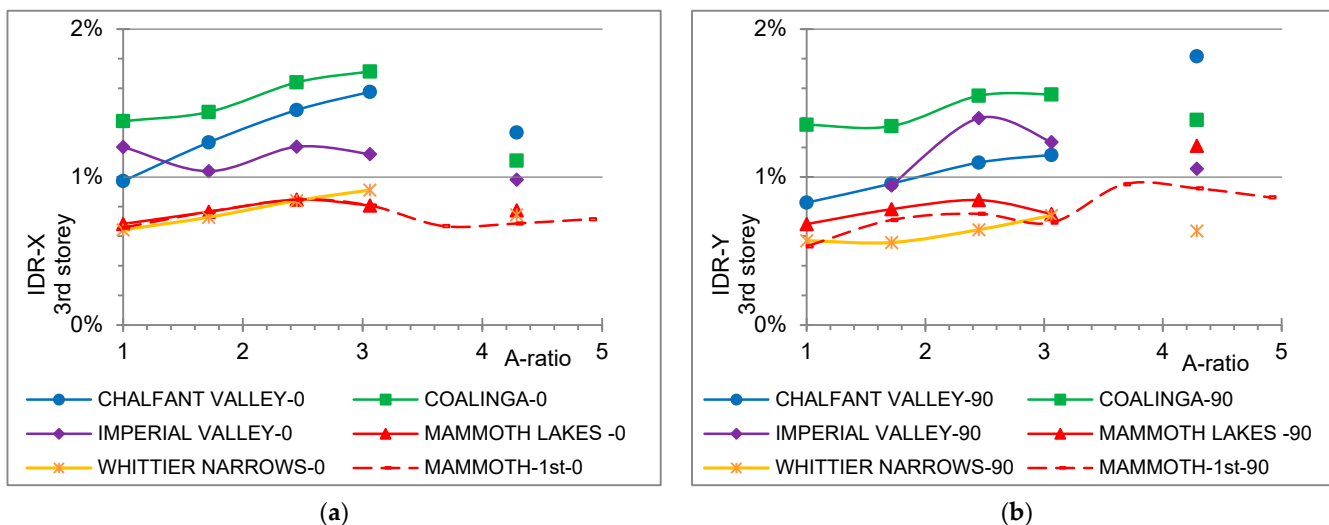


Figure 16. (a) IDR-X,  $\theta = 0^\circ$ , and (b) IDR-Y,  $\theta = 45^\circ$ , 3rd storey.

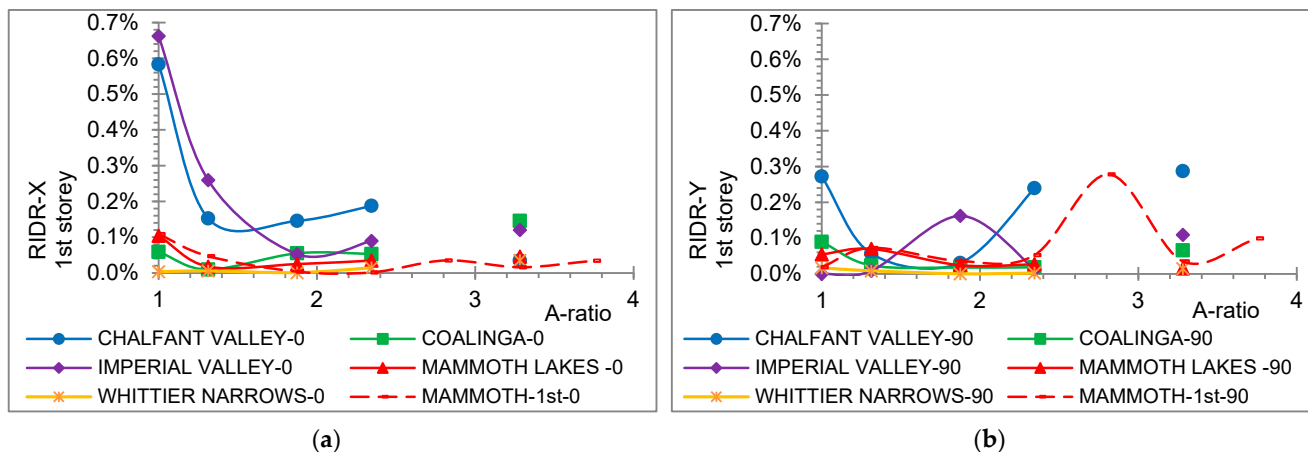


Figure 17. (a) RIDR-X,  $\theta = 0^\circ$ , and (b) RIDR-Y,  $\theta = 90^\circ$ , 1st storey.

At the 1st storey, the RIDR-Y with  $\theta = 90^\circ$  shows small values in the range of 0~0.29%, within the LS level [35] for all wall sections (Figure 17b). Gaps in the RIDR-Y plotline of Figure 17b represent building deficiency for A-ratio = 2.81 and A-ratio = 3.75, similar to Figure 17a. Greater RIDR-Y values tend to be observed for the Chalfant Valley earthquake and smaller ones for the Whittier Narrows earthquake (Figure 17b). For the Mammoth-1st excitation, the RIDR-X with  $\theta = 0^\circ$  varies in the range of 0~0.3% and the RIDR-Y,  $\theta = 90^\circ$ , varies in the range of 0~0.28% for all wall sections (Figure 17a,b), while building failures are not observed for this excitation in contrast with the entire Mammoth sequential excitation.

The RIDR-X at the 2nd storey,  $\theta = 0^\circ$ , presents a value range of 0~0.4% within the LS level [35] with higher values for the Chalfant Valley earthquake (Figure 18a). Relatively small values of RIDR-X, less than 0.07%, are observed for the excitations of Whittier Narrows and Mammoth-1st (Figure 18a).

At the 2nd storey, the RIDR-Y,  $\theta = 45^\circ$ , varies in the range of 0~0.25% (Figure 18b), with higher values for the Chalfant Valley earthquake and lower ones for the Whittier Narrows earthquake. The plotlines of RIDR-X and RIDR-Y are discontinued for specific wall sections, i.e., A-ratio = 2.81 and A-ratio = 3.75, due to building failure for the sequential excitations, as previously shown.

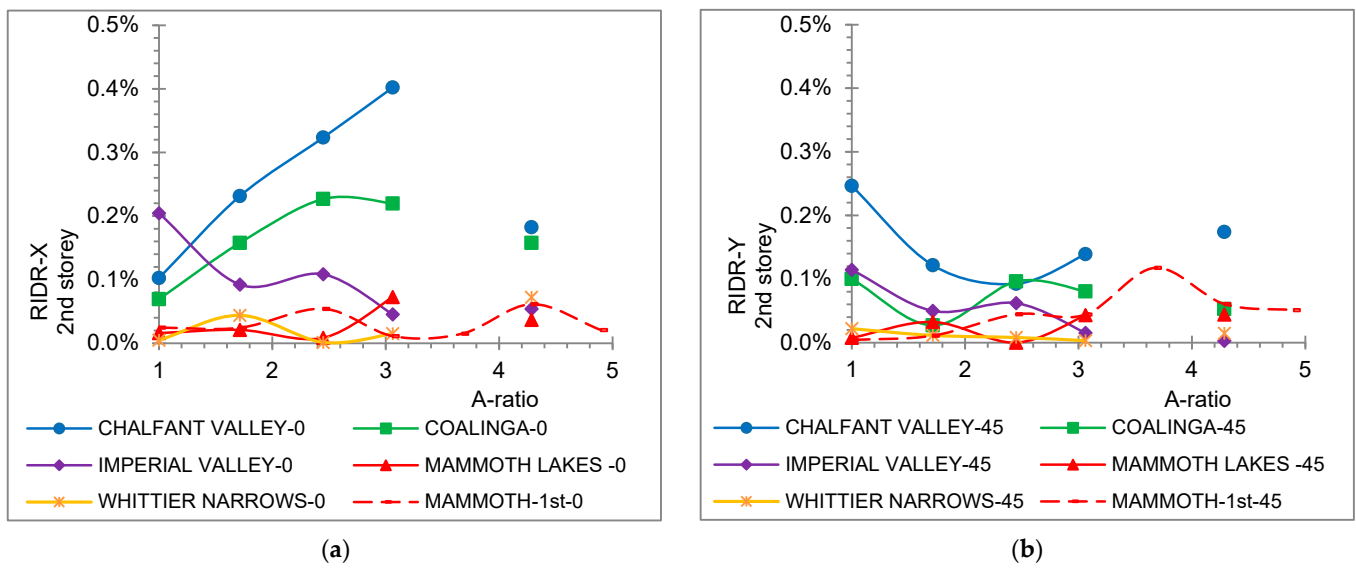


Figure 18. (a) RIDR-X,  $\theta = 0^\circ$ , and (b) RIDR-Y,  $\theta = 45^\circ$ , 2nd storey.

At the 3rd storey, the RIDR-X,  $\theta = 0^\circ$ , increases variably for greater wall sections in the range of 0~0.4% (Figure 19a), within the LS level [35]. At the same storey, the RIDR-Y,  $\theta = 45^\circ$ , increases variably with a greater A-ratio in the range of 0~0.25%, which is included in the LS level [35]. Similarly to the lower storeys, gaps in the RIDR plotlines are noticed for the specific wall sections, 150/30 cm and 200/30 cm, due to building deficiency for the sequential excitations, while the results of the Mammoth-1st, which is the single-event excitation, are fully plotted, indicating no failure (Figure 19a,b).

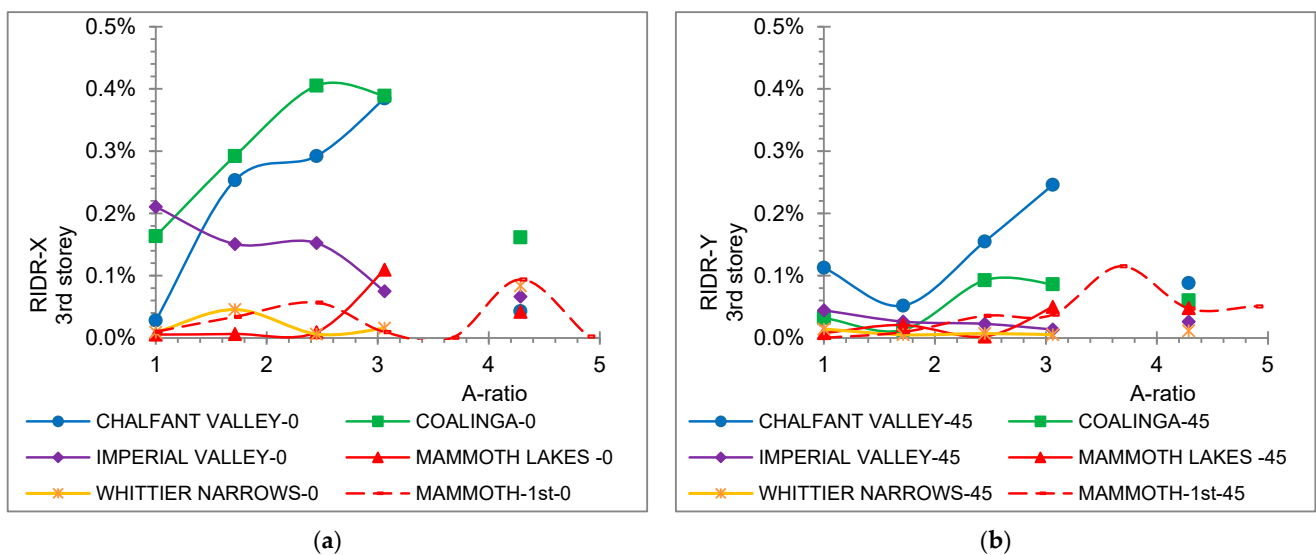


Figure 19. (a) RIDR-X,  $\theta = 0^\circ$ , and (b) RIDR-Y,  $\theta = 45^\circ$ , 3rd storey.

The RIDR plots at the 1st storey (Figure 17) have a smaller general range of values by 50% in X and 30% in Y compared to the second (Figure 18) and third storeys (Figure 19), with the aforementioned exception of the symmetrical building. The RIDR plots in the 2nd and 3rd storeys have comparable values in the horizontal axes. Although the general plot values of RIDR (Figures 17–19) are acceptable within the LS performance level [35], some local building failures are observed only for sequential excitations.

At the 1st storey,  $\theta = 45^\circ$ , the PFA/PGA-X shows greater values for greater wall sections with a narrow value field for all excitations in the range of 1.89~2.89 and a maximum value

of 3.82 for the Mammoth Lakes excitation (Figure 20a). Smaller values of PFA/PGA-X are observed for the Mammoth-1st excitation (Figure 20a) and greater ones for the Whittier Narrows and Imperial Valley sequential excitations.

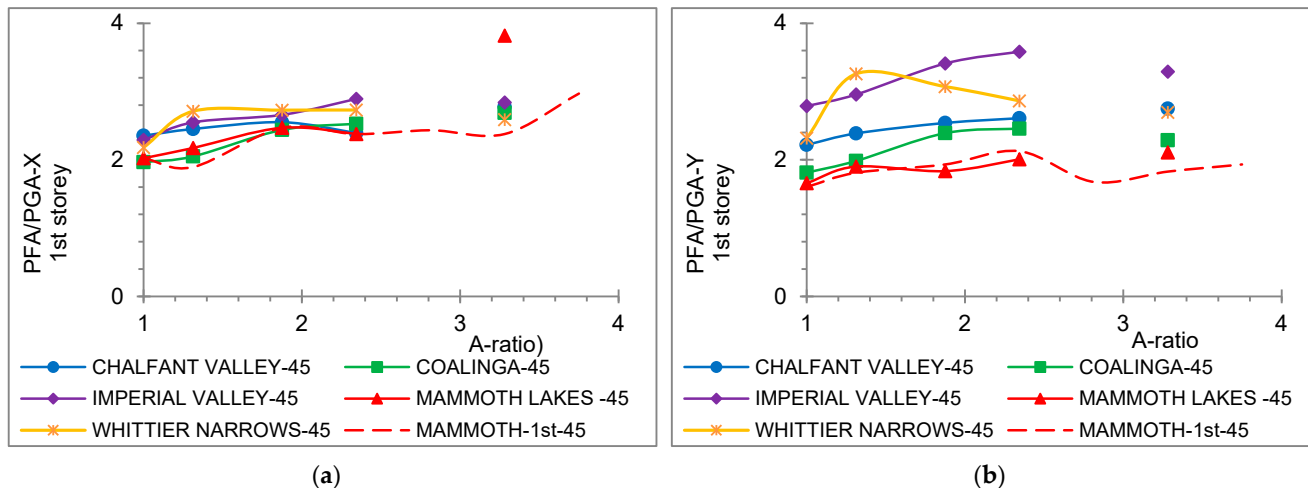


Figure 20. (a) PFA/PGA-X,  $\theta = 45^\circ$ , and (b) PFA/PGA-Y,  $\theta = 45^\circ$ , 1st storey.

At the same storey, the PFA/PGA-Y plotlines increase variably with an increase in the A-ratio, in the range of 1.83~3.58 (Figure 20b), with lower values for the Mammoth-1st excitation and higher values for the Imperial Valley sequence. The discontinuities of the PFA/PGA-X and PFA/PGA-Y plotlines represent building failure for the wall sections of 150/30 cm and 200/30 cm for the sequential earthquakes, which is not observed for the single-event excitation of Mammoth-1st (Figure 20a,b).

At the 2nd storey with  $\theta = 45^\circ$ , the PFA/PGA-X increases for greater wall sections in the range of 1.48~3.4, with bigger values for the Chalfant Valley earthquake and lower ones for the Coalinga (Figure 21a). In Figure 21b, the PFA/PGA-Y varies with a slightly increasing tendency for greater wall sections up to 1.5~3.25, with maximum values for the Imperial Valley sequence and smaller ones for the Mammoth Lakes.

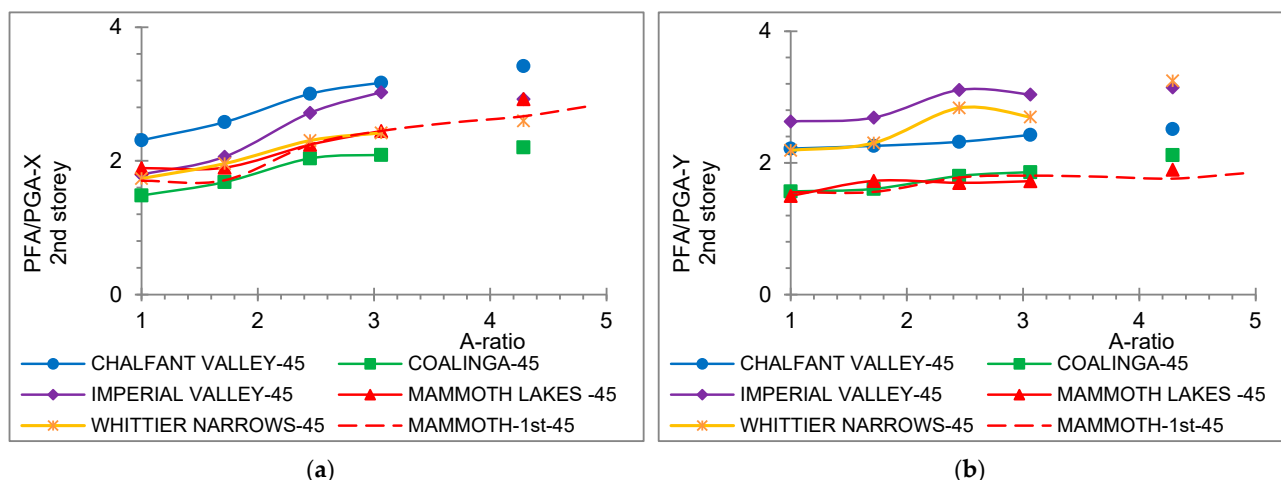


Figure 21. (a) PFA/PGA-X axis,  $\theta = 45^\circ$ , and (b) PFA/PGA-Y,  $\theta = 45^\circ$ , 2nd storey.

At the 3rd storey, the PFA/PGA-X,  $\theta = 45^\circ$ , increases almost linearly for greater A-ratios up to 2.1~4.6, with bigger values for the Chalfant Valley excitation and lower ones for the Coalinga (Figure 22a). On the Y-axis, for the same storey with  $\theta = 45^\circ$ , the PFA/PGA increases slightly for greater A-ratios up to 1.9~4.2 (Figure 22b), showing bigger values for the Imperial Valley earthquake and smaller values for the Mammoth-1st excitation.

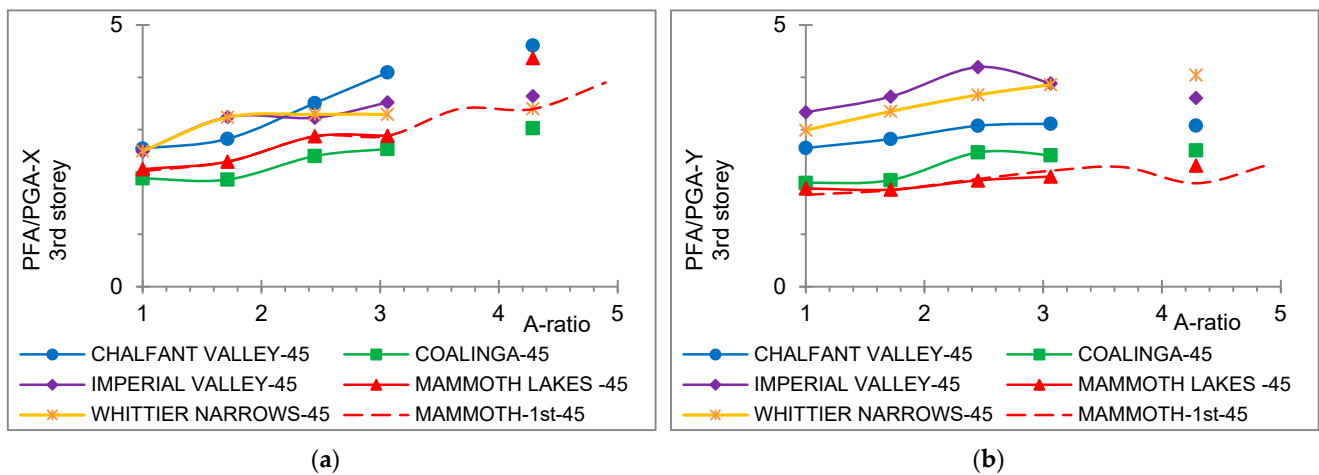


Figure 22. (a) PFA/PGA-X,  $\theta = 45^\circ$ , and (b) PFA/PGA-Y,  $\theta = 45^\circ$ , 3rd storey.

The PFA/PGA-X plot presents a higher range at the 2nd storey by 15% in reference to the 1st one and by 25% at the third storey referenced to the second one (Figures 20a, 21a and 22a). The PFA/PGA-Y plots show 11% lower values at the second storey in reference to the first one and 26% higher values at the third storey compared to the second one. Thus, the dimensionless peak floor acceleration ratio tends to increase strongly for higher storeys. At the plots of PFA/PGA at the horizontal axes of the 2nd and 3rd storeys (Figures 21 and 22), gaps in the plotlines are observed for the greater wall sections, such as for 150/30 cm and 200/30 cm, similarly to the 1st storey (Figure 20a,b), indicating building failure due to extreme deformations much over the acceptable limits of the seismic performance levels [35], for the sequential excitations. Therefore, a tendency appears that buildings with wall sections bigger than the wall limit considering the seismic design by [2,27] are vulnerable to sequential excitations compared to single-event ones.

For the three-storey framed structures, the elastoplastic hinges tend to present behaviour acceptable by the limits of [2,27] for most wall sections for the cases of sequential earthquakes (Figure 23a,b, Figure 24a,b and Figure 25a–c), as well as for the single-event excitation of Mammoth-1st (Figures 23c and 24c). Regarding the symmetrical three-storey building, more hinges tend to behave nonlinearly for the excitation of Chalfant Valley with  $\theta = 0^\circ$  (Figure 23a), less for the excitation of Mammoth Lakes with  $\theta = 90^\circ$  (Figure 23b), and even less for the single-event excitation of Mammoth-1st with  $\theta = 90^\circ$  (Figure 23c).

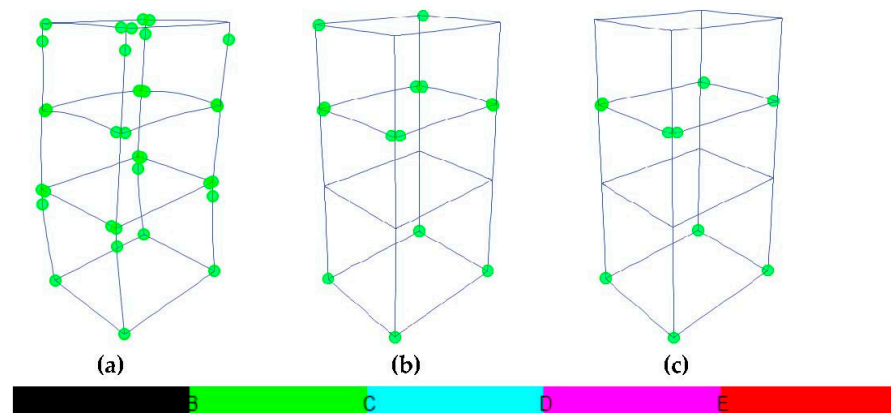
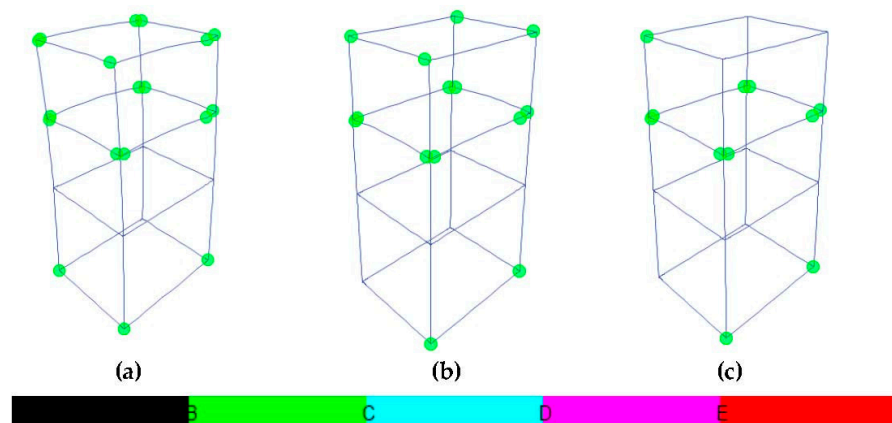
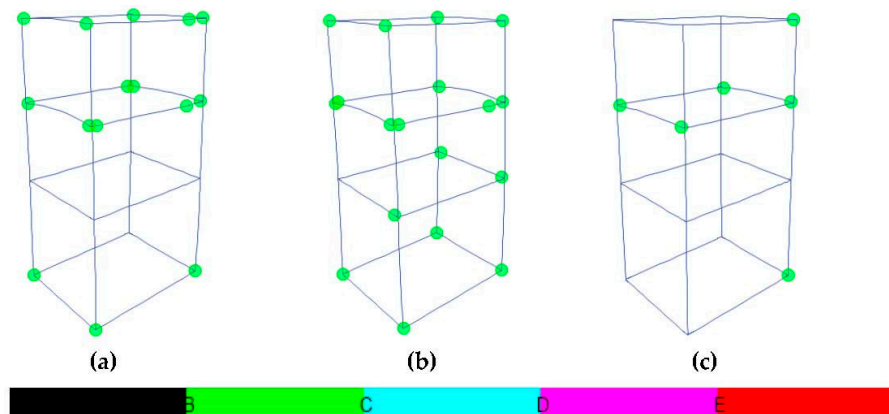


Figure 23. Hinge formation of the 3-storey symmetric frame; (a) Chalfant Valley with  $\theta = 0^\circ$ , (b) Mammoth Lakes with  $\theta = 90^\circ$ , and (c) the 1st part of Mammoth Lakes with  $\theta = 90^\circ$ .



**Figure 24.** Hinge formation of the 3-storey frame with wall section 125/30 cm for (a) Coalinga with  $\theta = 0^\circ$ , (b) Mammoth Lakes with  $\theta = 45^\circ$ , and (c) the 1st part of Mammoth Lakes with  $\theta = 45^\circ$ .



**Figure 25.** Hinge formation of the 3-storey frame with wall section 175/30 cm for (a) Coalinga with  $\theta = 45^\circ$ , (b) Imperial Valley with  $\theta = 45^\circ$ , and (c) Whittier Narrows with  $\theta = 90^\circ$ .

Concerning the symmetrical three-storey model with a wall section of 125/30 cm, similar hinge behaviour is presented for the earthquakes of Coalinga with  $\theta = 0^\circ$  and Mammoth Lakes with  $\theta = 45^\circ$ , where the hinges of the higher storeys tend to behave in a nonlinear way in contrast to the lower storeys (Figure 24a,b). For the three-storey structure with 125/30 cm wall section, regarding the Mammoth-1st excitation with  $\theta = 45^\circ$ , the majority of hinges tend to behave linearly (Figure 24c).

Regarding the three-storey frames with a wall section of 175/30 cm, more hinges are observed to behave inelastically for the Imperial Valley earthquake with  $\theta = 45^\circ$  and less for the Whittier Narrows earthquake with  $\theta = 90^\circ$  (Figure 25). Regarding the same frame, the nonlinear hinge behaviour tends to be observed at higher storeys, such as the building top and the top of the second floor, as well as at the column base (Figure 25), similar to previous plots (Figures 23 and 24). Additionally, the shear limit of [35] was not overpassed at the hinges of the considered one- and three-storey buildings, following the guidelines of the regulations [2,27,35].

#### 4. Conclusions

This research work aims to explore the elastoplastic behaviour of framed structures by reinforced concrete under sequential ground excitations, also considering one single-event ground excitation for comparison reasons. Low-rise one-storey and three-storey building models are analyzed by dynamic analysis. A simple geometrical cross-section ratio is used to account for the relative imbalance of the vertical members. The comparison of the dynamic results is performed through unitless quantities to offer more even-handed outcomes. Obviously, the role of symmetry or asymmetry is identified here regarding the

performance of reinforced concrete framed structures forced to multiple ground excitations. Based on the present analysis findings, the following remarks are plausible.

- (a) The IDR plot range tends to increase for greater wall sections while, in most cases, being within the acceptable limits of the seismic performance levels for RC structures.
- (b) The RIDR response plots have general values in the tolerable limits of the current seismic codes. A variable plot RIDR is observed, tending to increase for bigger wall sections. The RIDR tends to generally decrease for higher storeys. However, local increased RIDR values may imply a building deficiency needing to be examined by the rest of the response parameters.
- (c) The PFA/PGA ratio tends to increase for bigger wall sections, as well as for higher storeys, of the considered RC buildings.
- (d) The elastoplastic hinge formation shows that more intense nonlinear hinge behaviour is observed at the building top and higher storeys of the RC three-storey buildings subjected to sequential earthquakes.
- (e) The symmetrical one-storey RC buildings are vulnerable to sequential earthquakes as opposed to single-event ground excitation. Meanwhile, a similar sensitivity to sequential earthquakes is observed in the asymmetrical three-storey reinforced concrete framed structures with great wall sections, such as cross-sections exceeding the “wall” limitation of the applicable seismic regulations.
- (f) The consideration of single-event excitation underestimates the dynamic response of the examined structures by showing smaller response quantities as compared to the ones for the corresponding sequential earthquake.
- (g) The earthquake incidence angle of  $45^\circ$  appears to be more detrimental in the dynamic behaviour of the framed models compared to angles  $0^\circ$  and  $90^\circ$ , which are also important for consideration in the analysis.

The role of symmetry or asymmetry is found here to be important in the earthquake response of ordinary reinforced concrete framed models. Judging from previous remarks, a selection of wall sections smaller or even up to the “wall” limitation of the existing seismic regulations is suggested to enhance the resistance of reinforced concrete framed structures to sequential earthquakes.

**Funding:** This research received no external funding.

**Data Availability Statement:** Data are contained within this article.

**Conflicts of Interest:** The author declares no conflict of interest.

## References

1. Bento, R.; De Stefano, M.; Köber, D.; Zembaty, Z. *Seismic Behaviour and Design of Irregular and Complex Civil Structures IV*, 1st ed.; Springer Nature: Cham, Switzerland, 2022. [[CrossRef](#)]
2. Eurocode 8 (EC8). *Design of Structures for Earthquake Resistance—Part 1: General Rules, Seismic Actions and Rules for Buildings, Part 3: Strengthening and Repair of Buildings, Part 5: Foundations, Retaining Structures and Geotechnical Aspects. Part 6: Towers, Masts and Chimneys*; European Committee for Standardization: Brussels, Belgium, 2004.
3. Rutenberg, A. *Nonlinear Seismic Analysis and Design of Reinforced Concrete Buildings*, 1st ed.; Fajfar, P., Krawinkler, H., Eds.; Elsevier Science Publishers Ltd.: Essex, UK, 1992; pp. 328–355.
4. Das, P.K.; Dutta, S.C.; Datta, T.K. Seismic behavior of plan and vertically irregular structures: State of art and future challenges. *Nat. Hazards Rev.* **2021**, *22*, 04020062. [[CrossRef](#)]
5. Askouni, P.K.; Karabalis, D.L. SSI effects on the redistribution of seismic forces in one-storey R/C buildings. *Earthq. Struct.* **2021**, *20*, 261–278. [[CrossRef](#)]
6. Askouni, P.K.; Karabalis, D.L. SSI influence on the seismic response of asymmetrical small, low-rise R/C buildings. *Structures* **2021**, *32*, 1355–1373. [[CrossRef](#)]
7. Askouni, P.K.; Karabalis, D.L. The Modification of the Estimated Seismic Behaviour of R/C Low-Rise Buildings Due to SSI. *Buildings* **2022**, *12*, 975. [[CrossRef](#)]

8. Xing, B.; Lumantarna, E.; Lam, N.T.; Menegon, S. Torsional Rigidity of Asymmetrical Multi-Storey Reinforced Concrete Buildings. In Proceedings of the 2021 Australian Earthquake Engineering Society Virtual Conference, Virtual, 25–26 November 2021; Available online: <https://aees.org.au/wp-content/uploads/2022/02/24-Bin-Xing.pdf> (accessed on 10 September 2022).
9. Hatzigeorgiou, G.D.; Beskos, D.E. Inelastic displacement ratios for SDOF structures subjected to repeated earthquakes. *Eng. Struct.* **2009**, *31*, 2744–2755. [[CrossRef](#)]
10. Hatzigeorgiou, G.D. Behavior factors for nonlinear structures subjected to multiple near-fault earthquakes. *Comput. Struct.* **2010**, *88*, 309–321. [[CrossRef](#)]
11. Hatzigeorgiou, G.D. Ductility demand spectra for multiple near-and far-fault earthquakes. *Soil Dyn. Earthq. Eng.* **2010**, *30*, 170–183. [[CrossRef](#)]
12. Hatzigeorgiou, G.D.; Liolios, A.A. Nonlinear behaviour of RC frames under repeated strong ground motions. *Soil Dyn. Earthq. Eng.* **2010**, *30*, 1010–1025. [[CrossRef](#)]
13. Hatzivassiliou, M.; Hatzigeorgiou, G.D. Seismic sequence effects on three-dimensional reinforced concrete buildings. *Soil Dyn. Earthq. Eng.* **2015**, *72*, 77–88. [[CrossRef](#)]
14. Lazaridis, P.C.; Kavvadias, I.E.; Demertzis, K.; Iliadis, L.; Vasiliadis, L.K. Structural Damage Prediction of a Reinforced Concrete Frame under Single and Multiple Seismic Events Using Machine Learning Algorithms. *Appl. Sci.* **2022**, *12*, 3845. [[CrossRef](#)]
15. Loulelis, D.; Hatzigeorgiou, G.D.; Beskos, D.E. Moment resisting steel frames under repeated earthquakes. *Earthq. Struct.* **2012**, *3*, 231–248. [[CrossRef](#)]
16. Mahat, P.; Pradhan, P.; Adhikari, R.; Furtado, A.; Gautam, D.; Rupakhety, R. Seismic Sequence Vulnerability of Low-Rise Special Moment-Resisting Frame Buildings with Brick Infills. *Appl. Sci.* **2022**, *12*, 8231. [[CrossRef](#)]
17. Fujii, K. Peak and Cumulative Response of Reinforced Concrete Frames with Steel Damper Columns under Seismic Sequences. *Buildings* **2022**, *12*, 275. [[CrossRef](#)]
18. Konstandakopoulou, F.; Konstantinidou, M.; Pnevmatikos, N.; Hatzigeorgiou, G.D. Safety and Performance of Offshore Platforms Subjected to Repeated Earthquakes. *Infrastructures* **2020**, *5*, 38. [[CrossRef](#)]
19. Tsourekas, A.; Athanatopoulou, A.; Kostinakis, K. Maximum mean square response and critical orientation under bi-directional seismic excitation. *Eng. Struct.* **2021**, *233*, 111881. [[CrossRef](#)]
20. Di Sarno, L.; Amiri, S.; Garakaninezhad, A. Effects of incident angles of earthquake sequences on seismic demands of structures. *Structures* **2020**, *28*, 1244–1251. [[CrossRef](#)]
21. Altunışık, A.C.; Kalkan, E. Earthquake incidence angle influence on seismic performance of reinforced concrete buildings. *Sigma J. Eng. Nat. Sci.* **2017**, *35*, 609–631.
22. Altunışık, A.C.; Kalkan, E. Investigation of Earthquake Angle Effect on Seismic Performance of Steel Bridges. *Steel Compos. Struct.* **2016**, *22*, 855. [[CrossRef](#)]
23. Cantagallo, C.; Camata, G.; Spacone, E. The effect of the earthquake incidence angle on seismic demand of reinforced concrete structures. In Proceedings of the 15th World Conference on Earthquake Engineering, Lisboa, Portugal, 24–28 September 2012.
24. Weaam, A.; Craifaleanu, I.G. A Combined-Index Study on the Influence of Earthquake Incidence Angle on the Seismic Performance of Reinforced Concrete Plan-Asymmetric Buildings. *Model. Civ. Environ. Eng.* **2021**, *16*, 40–54. [[CrossRef](#)]
25. Magliulo, G.; Maddaloni, G.; Petrone, C. Influence of earthquake direction on the seismic response of irregular plan RC frame buildings. *Earthq. Eng. Eng. Vib.* **2014**, *13*, 243–256. [[CrossRef](#)]
26. Bosco, M.; Ghersi, A.; Marino, E.M.; Rossi, P.P. Comparison of nonlinear static methods for the assessment of asymmetric buildings. *Bull. Earthq. Eng.* **2013**, *11*, 2287–2308. [[CrossRef](#)]
27. Eurocode 2 (EC2). *Design of Concrete Structures—Part 1-1: GENERAL Rules and Rules for Buildings*; European Committee for Standardization (CEN): Brussels, Belgium, 2004.
28. Eurocode 1 (EC1). *Actions on Structures—Part 1-1: General Actions, Densities, Self-Weight, Imposed Loads for Buildings*; European Committee for Standardization (CEN): Brussels, Belgium, 2001.
29. Pacific Earthquake Engineering Research Center (PEER): Strong Motion Database. Available online: <https://ngawest2.berkeley.edu/> (accessed on 10 September 2022).
30. ETABS. *Integrated Building Design Software*; Computers and Structures Inc. CSI: Berkeley, CA, USA, 2015.
31. Sfakianakis, M.G.; Fardis, M.N. Nonlinear finite element for modeling reinforced concrete columns in three-dimensional dynamic analysis. *Comput. Struct.* **1991**, *40*, 1405–1419. [[CrossRef](#)]
32. Sfakianakis, M.G. Computation of Yield and Failure Surfaces for Biaxial Bending with Axial Force of Reinforced Concrete Sections with Jackets. In Proceedings of the 15 WCEE2012, Lisbon, Portugal, 24–28 September 2012.
33. Fardis, M.N. *Seismic Design, Assessment and Retrofitting of Concrete Buildings: Based on EN-Eurocode 8*, 1st ed.; Springer: Berlin, Germany, 2009.
34. Wilson, E.L. *Three-Dimensional Static and Dynamic Analysis of Structures*; Computers and Structures Inc.: Berkeley, CA, USA, 2002.
35. FEMA-356. *Prestandard and Commentary for the Seismic Rehabilitation of Buildings*. Washington, D.C.: Federal Emergency Management Agency, U.S.A; 2000. Available online: <https://www.nehrp.gov/pdf/fema356.pdf> (accessed on 10 September 2022).

36. Petrone, C.; Magliulo, G.; Cimmino, M.; Manfredi, G. Evaluation of the seismic demand on acceleration sensitive nonstructural components in RC frame structures. In Proceedings of the Second European Conference on Earthquake Engineering and Seismology, Istanbul, Turkey, 25–29 August 2014.
37. *Greek Interventions Regulation (KANEPE)*, 3rd ed.; Earthquake Planning and Protection Organization (EPPO): Athens, Greece, 2022; Available online: [https://www.oasp.gr/userfiles/%CE%9A%CE%91%CE%9D%CE%95%CE%A0%CE%95\\_3%CE%B7%20%CE%91%CE%BD%CE%B1%CE%B8%CE%B5%CF%8E%CF%81%CE%B7%CF%83%CE%B7.pdf](https://www.oasp.gr/userfiles/%CE%9A%CE%91%CE%9D%CE%95%CE%A0%CE%95_3%CE%B7%20%CE%91%CE%BD%CE%B1%CE%B8%CE%B5%CF%8E%CF%81%CE%B7%CF%83%CE%B7.pdf) (accessed on 10 September 2022). (In Greek)

**Disclaimer/Publisher’s Note:** The statements, opinions and data contained in all publications are solely those of the individual author(s) and contributor(s) and not of MDPI and/or the editor(s). MDPI and/or the editor(s) disclaim responsibility for any injury to people or property resulting from any ideas, methods, instructions or products referred to in the content.